

# A Model for Calculation of Magnetron Performance

J. RODNEY M. VAUGHAN

**Abstract**—A simplified model of the space charge in a magnetron is proposed, and the performance of the magnetron is calculated; the method differs from that of Welch in the space charge density assigned to the “spokes,” and from that of Hull in using energy conservation instead of the principle of induction to identify the operating point. The method is tested by applying it to four known magnetrons, covering a wide range of frequencies, operating voltages and power levels. In all four cases the method predicts the output power correctly within  $\pm 0.5$  dB, and the voltage within  $\pm 2$  percent, at the nominal operating current and field. It also predicts the frequency pushing, and provides information on the relative phase of the spokes, and other parameters. The spoke phase is found to be always within the range  $-20^\circ$  to  $-60^\circ$ .

## I. INTRODUCTION

**A**NALYSES of the microwave magnetron have been published at intervals over the past 30 years and have fallen mainly into the following three classes:

- 1) hydrodynamic theories [1], [2] that have been mainly small-signal approaches;
- 2) discrete particle calculations [3], [4] that have generally shown chaotic electron motions in a fairly well-defined hub, and trapezoidal “spokes” in the retarding RF phase region;
- 3) lumped-spoke analyses [5]–[8], of which the last was published in 1971, which treat the spoke as a single element of charge, ignoring all details of the individual trajectories—the induced currents are calculated and the problem is essentially reduced to circuit theory.

This paper is in the third category. Welch [5] originated this approach in 1953, deriving a qualitative explanation of frequency pushing, for both linear and circular format tubes, but taking account only of the currents induced by the tangential motion of the spokes. He obtained qualitative agreement with observation, but his calculated currents and powers were in error by factors up to about five. It will be shown that the lack of numerical agreement was due largely to the use of an incorrect expression for the space charge density in the spoke. In 1961, Hull [6], [7] allowed for the radial motion of the charge in the spoke, but confined his analysis to the linear model of the magnetron. Hull's equations were combined in such a way that the space-charge density was eliminated as a variable, but it is evident from notes in his thesis that he had the correct form in mind. In 1971, Azumi [8] combined Welch's and Hull's work, to produce a theory for cylindrical geometry incorporating both radial and tangential motions. Unfortunately, he has used Welch's expression for the space

charge density, and the resulting theory does not scale correctly.

The expression referred to is Welch's (37), a fairly complicated expression, which is not necessary to repeat in full. After discarding some small terms and simplifying, it becomes approximately

$$\rho = -4\pi\epsilon_0 f B / N \quad (1)$$

where  $f$  is the frequency,  $B$  the magnetic field, and  $N$  the number of resonators. Put in this form, the equation is easily seen to be untenable: it implies that if one doubled the number of resonators of a magnetron, (consequently doubling the anode diameter) keeping the frequency and other parameters the same, one would halve the space-charge density. But physically it is obvious that the only change seen by a single cell of the interaction space would be a minor change in the curvature effect, so that the spoke density would be only slightly different. Further, the expression varies directly with  $B$ , instead of the expected  $B^2$  dependence. The argument by which Welch obtained this equation was as follows: to maintain synchronism of an electron moving out to the anode radius, an additional tangential velocity is needed, and hence an additional dc voltage on the anode. In the presence of this increased voltage, there must be more space charge present to maintain space-charge-limited conditions at the cathode. This additional charge, distributed uniformly over the radial distance from the synchronous layer to the anode, leads to (1), and also ensures that electrons are synchronous at all intermediate radii.

This argument can be faulted because, first, it gives no spoke space charge at all for the linear model of the magnetron, in which the synchronous velocity is the same at the anode as at the synchronous layer, and second, it is not necessary to maintain dc synchronism at all levels: the RF forces are strong enough to force synchronism over a significant range of dc fields near the synchronous value. The space charge limitation at the cathode is maintained by a small change in the radius of the dense Brillouin hub of charge, rather than by a diffuse charge further out.

The actual charge density in the spoke is certainly complicated and nonuniform, but it seems reasonable to suppose that it is primarily governed by the density in the Brillouin hub, from which the spoke grows.

The purpose of this paper is to explore the possibilities of a model that uses Welch's criterion for the phase range in which a spoke will develop, but equates the density in the spoke to the Brillouin density immediately

below it, and adopts a triangular spoke shape suggested by the discrete particle calculations. This highly stylized model cannot be expected to give very accurate numerical results: the test is whether it will scale, without adjustment, over a wide range of known magnetron designs, which would indicate correct basic dependence on the tube parameters. It will be shown that this is the case.

## II. ANALYSIS

The physical model just described is illustrated in Fig. 1. We assume a conventional magnetron of  $N$  vanes, operating in the  $\pi$  mode, and the figure defines various dimensions. The angles  $\beta$  and  $\theta$  are phase angles, relative to the  $2\pi$  phase shift over one wavelength (two vanes) on the anode. The actual spatial angles subtended at the center of the magnetron are  $\beta/(N/2)$  and  $\theta/(N/2)$ . Superimposed on the magnetron outline is a representation of the voltages associated with the anode: the applied dc (or peak pulse) voltage, relative to the cathode, is  $V_a$ . This may be either less (as shown) or greater than the Hartree voltage  $V_H$ , given by

$$V_H = \frac{B\omega r_a^2}{N} (1 - \sigma^2) - \frac{2m\omega^2 r_a^2}{eN^2} V \quad (2)$$

where  $\omega$  is the radian frequency of the RF wave of rms amplitude  $V_{RF}$  riding on the dc voltage,  $\sigma = r_c/r_a$  and  $e$  and  $m$  have their usual values for the electron ( $e$  taken as positive).

Welch's great contribution was to recognize the connection between these three voltages and the angles  $\beta$  and  $\theta$ : the decreasing half-cycle of  $V_{RF}$  is the phase-focusing range, in which a spoke may form; but the electrons can only proceed to the anode within the phase range where the sum of the dc and RF voltages exceeds the Hartree voltage. Thus the phasewidth of the base of the spoke is the overlap  $\beta$  of these two phase ranges, given by

$$\beta = \arccos \left( \frac{V_H - V_a}{V_{RF}\sqrt{2}} \right). \quad (3)$$

Welch assumed the spoke to retain this width all the way to the anode, but this ignores the focusing effect of the RF fields, shown in numerous trajectory calculations. The adoption of a triangular spoke also involves an inconsistency, in that the radial velocity would have to be infinite at the vertex, and we shall modify this aspect later; for the moment, we assume a triangular spoke of width  $\beta$  (linear width  $\beta r_B/(N/2)$ ) at its base. The phase angle  $\theta$  between the center of gravity of this spoke and that zero of  $V_{RF}$  that is in the phase-focusing half-cycle, is given by

$$-\theta = \frac{\pi}{2} - \frac{\beta}{2} = \frac{1}{2} \arccos \left( \frac{V_H - V_a}{V_{RF}\sqrt{2}} \right). \quad (4)$$

The positive direction of  $\theta$  is in the direction of motion,

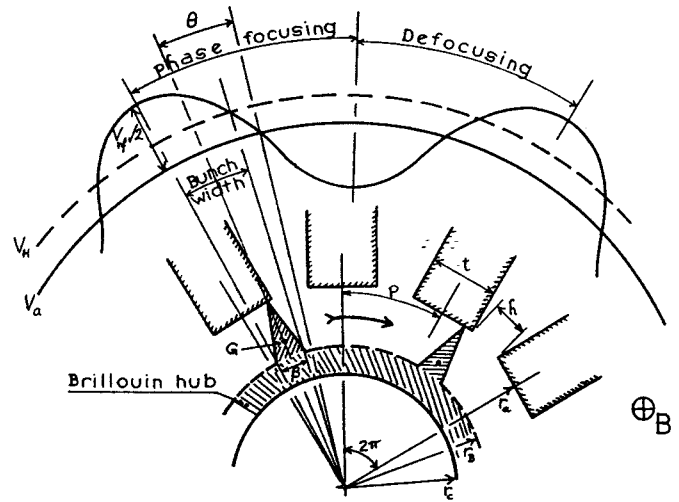


Fig. 1. Magnetron interaction space with hub and spoke model, anode voltage components and phase relations.

so that the value of  $\theta$  is normally negative, between  $-(\pi/2)$  and 0. Welch gave a discussion of possible instability if  $\theta$  becomes positive, while Hull indicated that the inclusion of the radial component of induced current would allow  $\theta$  to reach small positive values without instability. However, the numerical calculations from the present model indicate that  $\theta$  probably never comes further forward than about  $-20^\circ$  in practice, so that instability at  $0^\circ$  is academic.

The base of the spoke is taken at the Brillouin radius  $r_B$  given by

$$\frac{8mV_a}{eB^2r_c^2} = 2 \left\{ \left( \frac{r_B}{r_c} \right)^2 - \left( \frac{r_c}{r_B} \right)^2 \right\} \ln \frac{r_a}{r_B} + \left( \frac{r_B}{r_c} - \frac{r_c}{r_B} \right)^2. \quad (5)$$

While this equation does not have an explicit solution for  $r_B$ , the fact that the right-hand side increases monotonically as  $r_B$  is increased from  $r_c$  toward  $r_a$ , allows the equation to be solved unambiguously by simple iteration. The question whether the base of the bunch should be taken at the Brillouin radius given by (5) or at the synchronous radius given by

$$r_n = r_c \sqrt{1/(1 - 2m\omega/eB)} \quad (6)$$

is arguable. The ideal synchronous layer should appear as a perfect conductor to the RF fields, and act as the "supply plane" for electrons forming the spokes, but the cathode emission tends to maintain a dense hub out to  $r_B$ : this radius is slightly larger than  $r_n$  at normal operating voltages (increasing to  $r_a$  if the voltage is raised to cutoff). But the movies of computed trajectories made by the authors of [4] show no identifiable supply plane at all. The view taken here is that while the spoke may be drawn from the region of the synchronous radius, the only part of it that is effective in inducing current in the anode resonators is the part projecting above  $r_B$ . The

effect of this assumption is that as the dc voltage is raised,  $V_{RF}$  also increases, and the total charge in the spoke grows because of the increasing width  $\beta$  given by (3); but at higher voltages,  $\beta$  becomes nearly constant, while the height of the spoke  $r_a - r_B$  is now decreasing, and the spoke charge goes through a broad maximum and begins to decline.

The space charge density in the spoke is assumed to be uniform and equal to the value at the edge of the Brillouin hub:

$$\rho = \frac{\epsilon_0 e B^2}{m} \left\{ \left( 1 + \frac{r_c^4}{r_B^4} \right) / 2 \right\} \text{ cb/m}^3. \quad (7)$$

The total charge in the spoke, of axial length  $L$ , is

$$q = \frac{1}{2} \times \frac{\epsilon_0 e B^2}{m} \left\{ \left( 1 + \frac{r_c^4}{r_B^4} \right) / 2 \right\} \times r_B \beta / (N/2) \times (r_a - r_B) \times L \text{ cb.} \quad (8)$$

We now assume that for calculation of the interaction of this spoke with the circuit, we can treat this charge as being concentrated at the center of gravity  $G$  of the triangle: instead of integrating the effects of the RF fields over the whole area of the spoke, as Bayburin and Sobolev [9] have done, we evaluate the RF field *only* at  $G$ . For a sinusoidal field variation at the anode, the tangential component of field at  $G$  is (neglecting the interaction space curvature)

$$E_t = E_a \frac{\sinh(\frac{1}{3}\pi(r_a - r_B)/P)}{\sinh(\pi(r_a - r_B)/P)} \cos \theta \text{ V/m} \quad (9)$$

where  $E_a$  is the peak tangential field at the anode; since  $V_{RF}/\sqrt{2}$  is the peak RF voltage across the gap  $h$ , the amplitude of the fundamental component is

$$E_a = \frac{V_{RF}\sqrt{2}}{h} \times \frac{\sin(\pi h/P)}{\pi h/P}. \quad (10)$$

However, the field at the anode is stepped as shown in Fig. 2, because of the geometry of the vane tips; ordinarily one would add space harmonics to the fundamental to obtain a satisfactory approximation to this stepped wave, though most authors discuss the point and then decide to ignore all the space harmonics. However, as shown by Fig. 2, a substantial improvement in the representation for  $(\pi/2) < \theta < \pi/2$  can be made simply by using a  $\cos^2$  curve instead of a cosine curve: this would be completely invalid if  $\theta$  ever fell outside this range, as indicated by the dashed extension of the  $\cos^2$  curve, but we have already indicated that this does not occur. Thus, *in lieu* of adding any space harmonic components, we modify the fundamental with an extra factor  $\cos \theta$ . Hence

$$E_t = \frac{V_{RF}\sqrt{2}}{h} \times \frac{\sin(\pi h/P)}{\pi h/P} \times \frac{\sinh(\frac{1}{3}\pi(r_a - r_B)/P)}{\sinh(\pi(r_a - r_B)/P)} \cos^2 \theta \text{ V/m.} \quad (11)$$

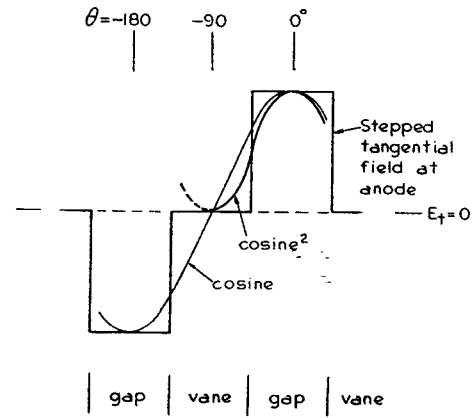


Fig. 2. Tangential field at anode face illustrating the use of a  $\cos^2$  curve to approximate the stepped field over a limited phase range, in lieu of adding space harmonics to the cosine fundamental.

The mean radial velocity of electrons in the spoke at  $G$  is determined by this tangential field as

$$v_r = E_t/B \text{ m/s.} \quad (12)$$

The cross-sectional area of the spoke, in the  $z-\theta$  plane at  $G$ , is

$$A = L \times \frac{2}{3} \times \frac{2r_B + r_a}{3} \times \frac{\beta}{N/2} \text{ m}^2. \quad (13)$$

Thus the current flowing outwards across this plane is

$$I_{\text{spoke}} = \rho v_r A \text{ A} \quad (14)$$

and, multiplying by the number of spokes  $N/2$ , we have the total current drawn by the magnetron:

$$I_{dc} = \rho \frac{E_t}{B} \times \frac{2L\beta}{3} \times \frac{2r_B + r_a}{3} \text{ A} \quad (15)$$

where  $\rho$  is given by (7),  $E_t$  by (11), and  $\beta$  by (3).

All of the quantities in (15) can be traced back through the preceding equations to the tube dimensions, the field  $B$ , the frequency  $\omega$ , and the voltages  $V_a$  and  $V_{RF}$ ; we thus have an expression for the current drawn by the magnetron for any assigned values of these voltages. It is not in explicit form, but the sequence of equations is straightforward for solution by iterative methods. However,  $V_a$  and  $V_{RF}$  cannot be assigned arbitrarily: for a given  $V_a$ , conservation of energy determines the value of  $V_{RF}$  and hence the RF operating level. To calculate this, we need to know the energy losses of the system.

We represent the anode resonant system as a parallel  $L-C$  circuit, shown in Fig. 3, shunted by two conductances,  $G_U$  representing the internal RF losses and  $G_E$  the externally connected load.  $L_1$  and  $C_1$  are an equivalent inductance and capacitance of a single cavity, such that  $\sqrt{L_1 C_1} = 1/2\pi f$ , and  $\sqrt{L_1/C_1} = Z_1$ , the characteristic impedance of a single resonator.  $Z_1$  may be measured by a perturbation experiment, or  $C_1$  may be estimated by methods given in Collins [10], and discussed in more detail by Hull [7]. Values of  $C/L$  are given by Collins for

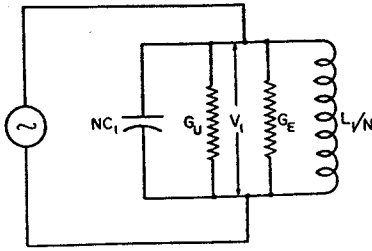


Fig. 3. Equivalent circuit of magnetron anode for  $\pi$ -mode operation.  $L_1$  and  $C_1$  are the inductance and capacitance of a single cavity.

a number of older magnetrons: these are equivalent to  $N^2 C_1 / L_1$  in the notation used here. If  $C_1$  is known, then  $Z_1 = 1 / \omega C_1$  and we define

$$Y_0 = N / Z_1 \quad (16)$$

$$G_E = Y_0 / Q_E \quad (17)$$

$$G_U = Y_0 / Q_U \quad (18)$$

$$G_L = Y_0 / Q_L \quad (19)$$

where  $Q_E$ ,  $Q_U$ , and  $Q_L$  have the usual meanings, and are measurable by standard cold test methods: alternatively,  $Q_E$  may be expressed in terms of the pulling figure  $f_p$ ; the theoretical relation is  $Q_E = 0.416 f / f_p$ , but a factor of 0.375 is found to give better numerical agreement, and was used in this work. The circuit efficiency is then

$$\eta_c = Q_L / Q_E \quad (20)$$

The output power is

$$P_E = V_{RF}^2 G_E \quad \text{W} \quad (21)$$

and the internal RF loss is

$$P_U = V_{RF}^2 G_U \quad \text{W} \quad (22)$$

The next source of energy loss is the bombardment of the vane tips, due to both tangential and radial components of velocity on impact. The tangential component could be as low as  $V_0$  (the synchronous velocity expressed in volts) if the trajectories were quite laminar, or as high as  $4V_0$  if full cycloiding were maintained right out to the anode (since collection always occurs at the top of the cycloidal arch, where the velocity is twice the mean velocity). Discrete-particle trajectory plots, in particular the movies made by the authors of [4], show that the motion is far from laminar, but the efficiency of typical magnetrons shows that the impact velocity cannot be near  $4V_0$  in most cases. We arbitrarily assign a tangential impact voltage

$$V_T = 1.6 V_0 \quad (23)$$

for strapped magnetrons, recognizing that this factor could be adjusted to force agreement on efficiency. The synchronous voltage  $V_0$  is given by

$$V_0 = 2 \frac{m}{e} (\omega r_a / N)^2 \quad \text{V} \quad (24)$$

In rising sun magnetrons, at fields within about 20 percent either side of the cyclotron resonance, the zero mode of the anode strongly excites the cycloidal component of motion, causing the well-known efficiency dip. The value of the cyclotron field  $B_c$ , including Boot's empirical correction factor for the circular geometry, is given by

$$B_c = \frac{m\omega}{e} (1 + 3/N) \quad \text{T} \quad (25)$$

At this field we should expect the tangential impact velocity (expressed as a voltage) to rise to about  $4V_0$ , since this is the velocity at the top of an ideal cycloid in the linear case. Far from the cyclotron resonance it should approach the value (23). An ad hoc formula that approximates this variation is

$$V_T = V_0 \times \{1.4 + 1 / (0.4 + 10 \times |B/B_c - B_c/B|)\} \quad \text{V} \quad (26)$$

We choose (23) if the magnetron is specified as being a strapped type, and (26) if it is a rising sun tube.

The radial component of velocity when the electron reaches the anode is

$$v_{ra} = \frac{E_a}{B} \cos \theta \quad \text{m/s} \quad (27)$$

or in volts

$$V_R = 2.84 \times 10^{-12} \left( \frac{E_a}{B} \cos \theta \right)^2 \quad \text{V} \quad (28)$$

This evaluation of the radial velocity is not strictly compatible with the triangular spoke model; it implies that we are now thinking of a trapezoidal spoke. However, comparison of (12) and (28), using typical numerical values, shows that the top width is normally less than 10 percent of the base, so the triangular model is not seriously compromised. The power dissipated at the vane tips is then

$$P_A = I_{dc} (V_T + V_R) \quad \text{W} \quad (29)$$

The present analysis gives no direct indication of back-heating of the cathode; but knowing that it occurs, and that it varies from about 5 percent of the input power at typical operating points, up to 50 percent or more at very low inputs, we represent it by an ad hoc expression

$$P_C = 0.04 I_{dc} V_a / \cos \theta \quad \text{W} \quad (30)$$

Hence the power balance equation for the tube is

$$I_{dc} V_a = P_E + P_U + P_A + P_C \quad (31)$$

in which all the quantities are now expressed in terms of  $V_a$ ,  $V_{RF}$  and the tube data.

For a given  $V_a$ , we find that the left-hand side of this equation increases almost linearly with  $V_{RF}$  [through the variation of  $I_{dc}$  given by (15)], while the  $P_E$  and  $P_U$  terms on the right increase with  $V_{RF}^2$ , by (21) and (22).

Thus, the equation can be solved unambiguously by a simple iteration on  $V_{RF}$ .

When the operating point has been found, we know the (negative) angle  $\theta$  by which the spokes lead the RF voltage; the frequency of excitation is therefore pushed from  $f$  to  $(1+\delta)f$  where

$$\delta = 0.5 \tan \theta / Q_L. \quad (32)$$

This expression ignores the pushing due to radial components of motion, which are in quadrature with the induction due to the dominant tangential motion. From Azumi's [8] equations (7) and (20), which this author believes to be correct except for the  $\rho$  term already discussed, we find the ratio of radial to tangential induction to be (in our notation)

$$R = \frac{4\sqrt{2}V_{RF} \cos \theta}{\pi N h f B(r_a - r_n)}. \quad (33)$$

Since  $\rho$  has dropped out of the ratio, the question of its value does not matter here. We have used an approximation to Welch's  $F(\alpha, N, R_a, R_n)$  in obtaining (33).

Consequently the effective phase angle for the induced current is not  $\theta$  but  $\theta - \arctan R$ , and (32) becomes

$$\delta = 0.5 \tan (\theta - \arctan R) / Q_L. \quad (34)$$

Equations (33) and (34) therefore yield the frequency pushing  $\delta f$ .

### III. NUMERICAL RESULTS

The foregoing equations have been used to calculate the performances of four widely different magnetrons:

- 1) 4J50, a high-power pulsed X-band magnetron.
- 2) ZM-5458, a low-voltage 915-MHz CW magnetron.
- 3) L-5001, a medium-voltage 2450-MHz ac-operated magnetron.
- 4) 35M30/LD505, a pulsed high-power millimeter-wave magnetron.

These tubes span ranges of more than 35 to 1 in both frequency and nominal operating voltage, 10 to 1 in magnetic field and 2.5 to 1 in number of vanes, so that they adequately test the scaling properties of this model.

To perform the calculations it is necessary to assemble the following data on each tube: anode diameter, anode length, number of vanes, vane tip thickness, cathode diameter, magnetic field, cold resonant frequency, pulling figure (or  $Q_E$ ), unloaded  $Q(Q_U)$ , cavity impedance (or capacitance). If the resonant frequency of the next higher mode is known, this can be used also to check when a Gauss line has reached the Hartree voltage for this mode, where a mode boundary may be expected.

The calculation is normally carried out not only at the specified magnetic field, but also at fields 25 percent higher and lower, to provide data for a complete  $V$ - $I$  chart in conventional form.

At each field value,  $V_a$  is first set to 0.8  $V_H$  and then incremented in small steps. At each step, the sequence of

equations through (31) is evaluated to determine whether a nonzero solution of (31) exists. There is always a solution with zero current and power, but the energy conservation method does not recognize that this solution becomes unstable above some voltage in the region of 0.9  $V_H$ , and there is then a nonzero solution also. This is found by starting  $V_{RF}$  at a value such that  $V_{RF}\sqrt{2}$  just exceeds  $|V_a - V_H|$ , so that enough current is drawn to bias (31) off the zero solution. If the right-hand side of (31) already exceeds the left, then the minimum operating voltage has not yet been reached, and  $V_a$  is incremented; if it does not, then  $V_{RF}$  is incremented until the nonzero solution of (31) is found. It is found to be sufficiently accurate (in relation to the other approximations that have been made) if the balancing value of  $V_{RF}$  is found within limits of  $\pm 0.005 V_a$ . This gives the operating point for the voltage  $V_a$ . In the process of finding it, we have already calculated a great deal of information about the power and charge distribution within the tube, and by now continuing through (34) we obtain the frequency pushing also.

The process of incrementing  $V_a$ , and thus moving out along the Gauss line, is continued until one of four possible limiting conditions is reached.

- 1)  $V_a$  reaches the Hull cutoff voltage.
- 2)  $V_a$  reaches the Hartree voltage for the next mode, if known.
- 3) The RF voltage significantly exceeds the anode voltage, a condition called "RF bottoming" by analogy with anode bottoming in a triode amplifier. The specific limit used is that the peak RF voltage not exceed the anode voltage by more than 22 percent, an empirical figure.
- 4) The RF focusing fields at the base of the spoke exceed the space charge repulsion forces, causing "spoke pinch-off."

The reality of spoke pinch-off is open to debate: if one considers the spoke to be squeezed at constant density, then such an instability should exist; but if the spoke is squeezed at constant total charge, it should not occur. Since constant density is a basic assumption of this model, a spoke pinch-off test is made at each  $V_a$ . The relevant forces are easily calculated from the analysis given already.

At low values of magnetic field the calculation usually terminates on a sloping boundary on the right due to either "mode boundary" or spoke pinch-off, while at high fields the Gauss lines run into a nearly horizontal boundary across the top due to RF bottoming; since this kind of dual boundary is quite often seen in magnetron performance charts, it is thought that RF bottoming is a real effect, though it is certainly an oversimplification to take it as a fixed percentage of  $V_a$ .

Fig. 4 is a calculated performance chart of the 4J50, and Table I is a sample calculation corresponding to the middle Gauss line of Fig. 4; before going into any detailed consideration of this table, we will establish its

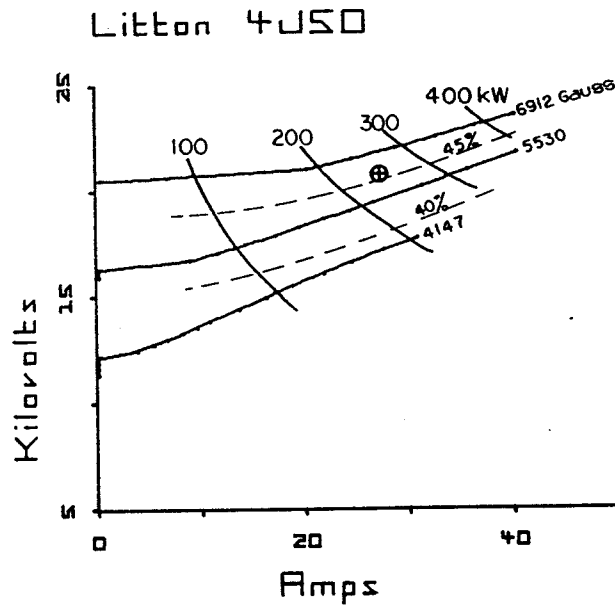


Fig. 4. Calculated performance chart of 4J50 magnetron. Tube parameters are given under Table I. ⊗ is Hull's operating point, 5530 G, 20.9 kV, 27.5 A, 232-kW output, 40.5-percent efficiency.

TABLE I

| $V_a$   | $I_{dc}$ | $P_E$        | $P_U$   | $P_A$       | $P_C$        | $\eta$     | $V_{rf}$ | $\theta$    | $\beta$     | $q$          | $r_B$      | $\delta f$    | Cath.             |
|---------|----------|--------------|---------|-------------|--------------|------------|----------|-------------|-------------|--------------|------------|---------------|-------------------|
| Voltage | Current  | Power Output | RF Loss | Anode Bbdt. | Back Heating | Efficiency | RF (rms) | Spoke Phase | Spoke Width | Spoke Charge | Hub Radius | Freq. Pushing | Current Density   |
| kV      | Amp      | kW           | kW      | kW          | kW           | %          | kV       | deg         | deg         | nanocb       | inch       | MHz           | A/cm <sup>2</sup> |
| 16.36   | 0        | 0            | 0       | 0           | 0            | -          | 0        | -           | -           | 0            | .124       | -             | 0                 |
| 16.75   | 9.0      | 66.6         | 28.5    | 45.3        | 9.8          | 44.3       | 8.2      | -51.7       | 76.6        | .836         | .124       | -22.3         | 7.7               |
| 17.14   | 11.7     | 88.2         | 37.9    | 60.3        | 12.5         | 44.4       | 9.5      | -50.0       | 80.0        | .867         | .124       | -20.8         | 10.1              |
| 17.53   | 14.3     | 110.6        | 47.4    | 75.6        | 15.2         | 44.4       | 10.6     | -48.7       | 82.6        | .888         | .124       | -19.8         | 12.3              |
| 17.92   | 17.2     | 136.7        | 58.7    | 93.6        | 18.3         | 44.5       | 11.8     | -47.7       | 84.7        | .889         | .125       | -19.0         | 14.8              |
| 18.31   | 19.5     | 157.7        | 67.7    | 108.5       | 20.9         | 44.4       | 12.6     | -46.9       | 86.3        | .899         | .125       | -18.3         | 16.7              |
| 18.70   | 21.9     | 181.2        | 77.9    | 125.0       | 23.7         | 44.4       | 13.5     | -46.2       | 87.7        | .907         | .126       | -17.7         | 18.8              |
| 19.09   | 24.4     | 207.5        | 89.2    | 143.4       | 26.6         | 44.5       | 14.5     | -45.5       | 88.9        | .912         | .126       | -17.2         | 20.9              |
| 19.48   | 26.7     | 230.9        | 99.3    | 160.7       | 29.4         | 44.4       | 15.3     | -45.0       | 90.0        | .916         | .126       | -16.7         | 22.9              |
| 20.26   | 31.4     | 280.6        | 120.8   | 199.6       | 35.4         | 44.1       | 16.8     | -44.1       | 91.9        | .913         | .127       | -16.5         | 26.9              |
| 21.04   | 35.7     | 328.8        | 141.5   | 238.4       | 41.2         | 43.8       | 18.2     | -43.3       | 93.4        | .922         | .128       | -16.4         | 30.6              |
| 21.81   | 40.4     | 381.3        | 164.2   | 284.5       | 47.8         | 43.4       | 19.6     | -42.6       | 94.8        | .913         | .128       | -16.3         | 34.6              |

Sample calculation for Litton 4J50 at 5530 Gauss, corresponding to the middle Gauss line in Fig. 5. Parameters:  $d_a = 0.344$ ,  $l_a = 0.257$ ,  $N = 16$ ,  $i = 0.035$ ,  $d_c = 0.224$ ,  $F_0 = 9396$  MHz,  $F_p = 8.7$  MHz,  $QV = 936$ ,  $Z_1 = 40 \Omega$ ,  $F(NB-1) = 11$  600-MHz strapped tube. Note: These parameters differ from those in Collins (10), which refer to a 4J50 of different manufacture. The calculated quantities are all pulse values. Average currents and powers are obtained by multiplying by the duty factor, typically 0.001. The table terminates at 21.81 kV because of "RF bottoming" ( $\sqrt{2} \times 19.6 > 1.22 \times 21.81$ , see text).

general validity by reviewing the performance charts of the other three magnetrons, shown in Figs. 5-7. On each chart a ⊗ indicates the actual (nominal) operating point, and the caption gives the measured data at this point. In the case of the 35M30/LD505 (Fig. 7), a larger number of Gauss lines was calculated, to show the effect of (26) in representing the efficiency dip region for a rising sun magnetron. Apart from this, the calculation procedure and the arbitrary constants used [e.g., in (23)] were identical in all four cases. Table II summarizes the discrepancies between the calculated and reported data at these operating points; these "errors" are some unknown combination of measurement errors

and inadequacies of the model. The iterations were carried far enough that arithmetical errors are probably small compared to either. The errors shown in Table II are both positive and negative, but show no "trend" with frequency or voltage or  $N$ ; we conclude that, while the model is not a precise one, it does scale correctly over a wide range of cases, and the arbitrary constants are reasonably well chosen. The overall accuracy of the model seems to be in the region of 10 percent, which is sufficient for many engineering purposes; it could surely be improved by adjustment of the constants to obtain agreement with really carefully taken data.

We can now return to Table I with some confidence

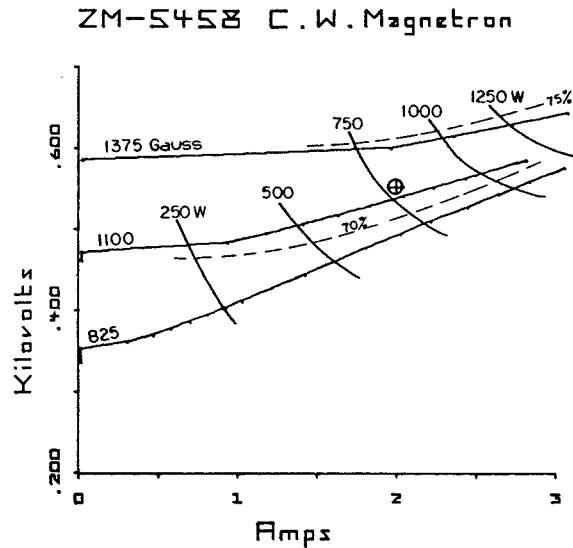


Fig. 5. Calculated performance chart of ZM-5458 915-MHz CW magnetron.  $\oplus$  is the actual operating point, 1100 G, 550 V, 2.0 A, 700-W output, 63.5-percent efficiency.

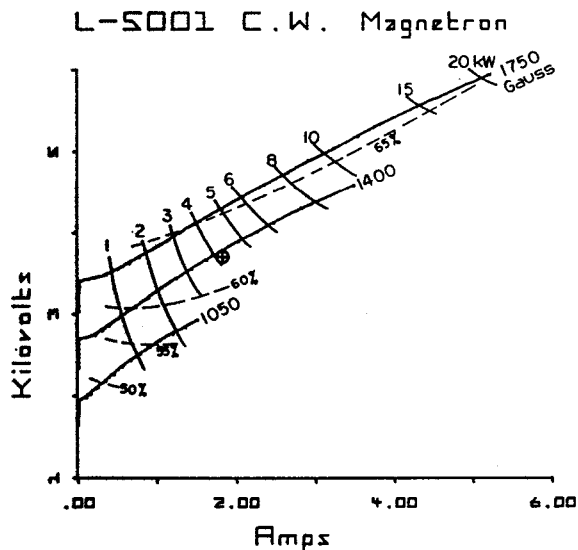


Fig. 6. Calculated performance chart of L-5001 2450-MHz ac magnetron.  $\oplus$  is the actual peak operating point, 1400 G, 3.75 kV, 1.8 A, 4.5-kW output, 66.5-percent efficiency.

that the mass of data it contains does have validity, at least at the 10-percent error level. The columns are not in the order of calculation, but in some kind of order of importance; the first three give the operating point and output power; the next three are useful for thermal calculations: the whole of  $P_A$  (multiplied by the duty factor) has to be conducted through the whole radial length of the vanes, and for strapped magnetrons at least half of  $P_V$  will originate in the straps and also require conduction through the vanes. The efficiency is seen to go through a broad maximum and start to decline, mainly because  $P_A$  is increasing faster than linearly. The most surprising column (to this writer) is the spoke phase  $\theta$ : less than  $10^\circ$  covers the whole Gauss line, and in the entire set of four magnetrons  $\theta$  never came further for-

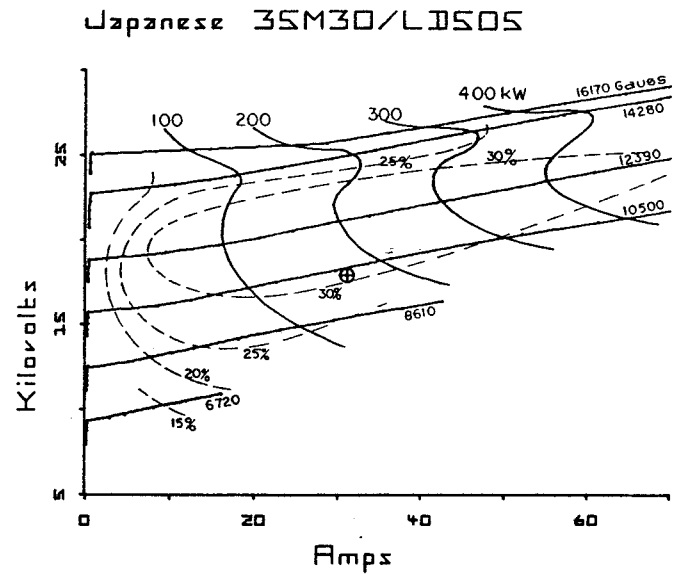


Fig. 7. Calculated performance chart of 35M30/LD505 high-power pulsed millimeter-wave magnetron [11].  $\oplus$  is the actual operating point, 10 500 G, 18.0 kV, 31 A, 180-kW output, 32-percent efficiency.

ward than  $-20^\circ$ , or further back than  $-60^\circ$ . This small range of  $\theta$  indicates the numerical difficulty to be expected in any analysis that uses  $\theta$  as the independent variable. To some extent the criticism of "small range" can also be leveled against the use of  $V_a$  as independent variable, but at least this has the merit of conforming closely to what one actually does when testing a tube.

The charge  $q$  in one spoke rises to a broad maximum as the spoke width increases, and then begins to decrease as the height ( $r_a - r_B$ ) decreases. In other tubes the decline is more pronounced than in the 4J50. The frequency pushing  $\delta f$  approaches a maximum, at which the pushing figure is zero; while this point is just beyond the calculated range for the 4J50, it is within the range for the other tubes. The cathode current density is given for information, but it plays no real part in the calculation: it is not used as a limit condition because much or all of it may be secondary emission [13].

The phase and frequency pushing data are plotted on the  $V$ - $I$  chart in Fig. 8, which emphasizes the narrow range of  $\theta$ . The absolute pushing is also plotted against the current in Fig. 9, together with Hull's calculated and measured curves. His measurements were carefully corrected for thermal effects, and show that the absolute pushing is predicted with useful accuracy by either method.

The data line in Table I at 19.48 kV, on which  $\theta = -45^\circ$ , represents operation at the Hartree voltage; for the 4J50, this is essentially at the normal operating point, but in most cases operation is above  $V_H$ . In all cases, however, the Gauss lines start well below the corresponding Hartree voltages, in accordance with Welch's theory that only the sum of  $V_a$  and  $V_{RF}\sqrt{2}$  must exceed  $V_H$ . The reduced performance charts in Collins [10] show an interesting division of opinion in

TABLE II

| Tube Type        | Frequency<br>GHz | Nom. Operating<br>Pt.<br>kV | Operating<br>Pt.<br>A | Field, Gauss |       |       | Power Output, kW |       |        | Efficiency, % |       |        |
|------------------|------------------|-----------------------------|-----------------------|--------------|-------|-------|------------------|-------|--------|---------------|-------|--------|
|                  |                  |                             |                       | Actual       | Calc. | Error | Actual           | Calc. | Error  | Actual        | Calc. | Error  |
| 4J50<br>(Litton) | 9.375            | 20.9                        | 27.5                  | 5530         | 6000  | +8.5% | 232              | 260   | +5dB   | 40.5          | 45.5  | +12.5% |
| ZM-5458          | .915             | .55                         | 2.0                   | 1100         | 1150  | +4.5% | .700             | .785  | +5dB   | 63.5          | 72    | +13.5% |
| L-5001           | 2.45             | 3.75                        | 1.8                   | 1400         | 1360  | -3%   | 4.5              | 4.2   | -.3dB  | 66.5          | 62    | -7%    |
| 35M30/<br>LD505  | 35.0             | 18.0                        | 31                    | 10500        | 10250 | -2.5% | 180              | 170   | -.25dB | 32            | 30    | -6.5%  |

Comparison of actual measured values with values at the same  $V$ - $I$  point calculated by this program, for four magnetrons. Actual values for the 4J50 are from [7, p. 117], and the corresponding conditions were used as input data in Fig. 4. Actual values for the 35M30/LD505 are from [11]. Others are from published commercial data. Calculated values are read by interpolation from Figs. 5-8.

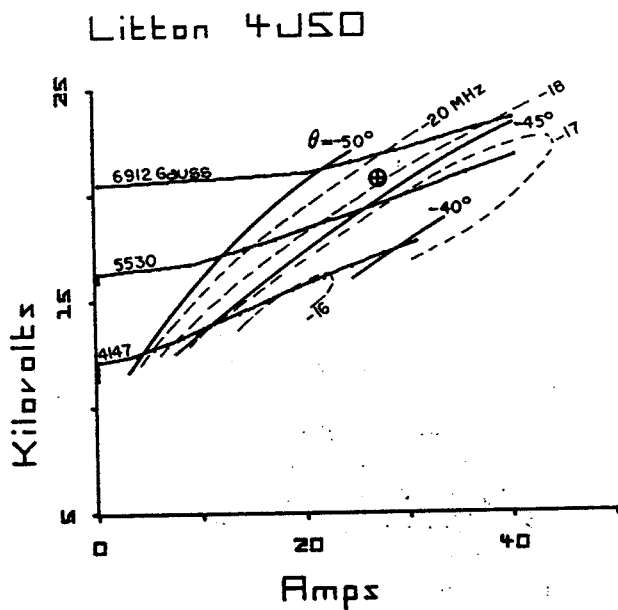


Fig. 8. Spoke phase and frequency pushing curves for 4J50. Note the small range of  $\theta$  that covers the whole working region. Zero pushing figure occurs where the tangent to a  $\delta f$  curve is parallel to the adjacent Gauss lines.

this respect: on each of them, the Gauss lines can be projected back to give the voltage at zero current, which can be expressed as a percentage of  $V_H$ . Fig. 10 is the rather skew histogram of these percentages for all the charts: it appears that the tall bar at 100 percent represents the work of one person or group who adjusted their data to fit the view that current flow must start at the Hartree voltage, while the roughly "normal" distribution from 82 to 95 percent represents plots (by another group) of actual data. A further example of a published reduced performance chart that has been so "adjusted" may be found in [12], the author of which would rather have remained anonymous.

IV. DEFICIENCIES OF THIS MODEL AND DIRECTIONS FOR FURTHER REFINEMENT

While it is clear that the Gauss lines should originate below  $V_H$ , the triangular spoke model tends to exaggerate the reduction and then to compensate with

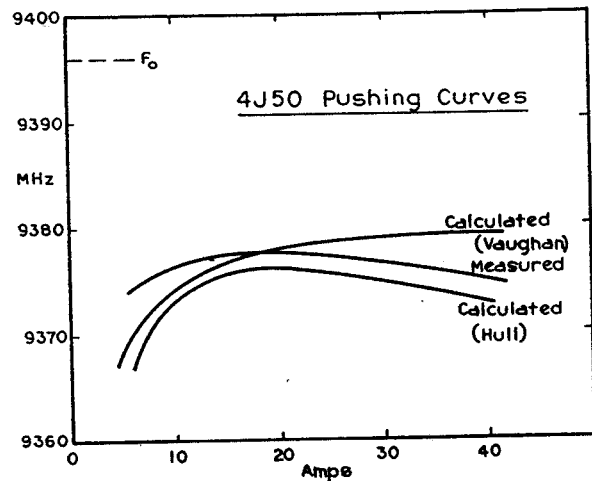


Fig. 9. Frequency pushing versus current for 4J50. Curve labeled "calculated (Vaughan)" is ( $f_0$ +column 13) of Table I. The measured and calculated values of Hull [7] are shown for comparison.

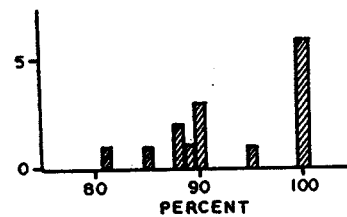


Fig. 10. Histogram of "reduced performance charts" in [10]. Abscissa is the ratio of "voltage at  $I=0$ " to  $V_H$ , averaged for all Gauss lines on the chart, expressed as a percentage. The ordinate is number of charts.

a dynamic impedance that is too high. The over-large reduction may be due to the fact that the model takes no account of the spreading of the excess fields: a combination of  $V_a$  and  $V_{RF}$  that exceeds the Hartree voltage at the anode does not necessarily exceed the Hartree field at the edge of the space charge hub.

The calculated dynamic impedance is strongly dependent on the value used for the cavity impedance or capacitance. This is one of the most difficult parameters either to measure or to calculate, so that it is hard to tell how much the too high slopes are due to deficiencies in the model, and how much to poor data.

The Gauss lines also show a distinct change of

slope between the first point at nonzero current and the remainder; that is, they imply an abrupt jump into oscillation rather than a continuous transition. This is qualitatively in agreement with observation on well-aligned tubes with good magnetic field uniformity: Fig. 11 is the actual V-I trace of an L-5001, showing substantial similarity to the middle line of Fig. 6, but the calculated jump becomes exaggerated at higher fields.

From Fig. 7 it can be seen that (26) models the efficiency dip fairly well, but the Gauss line at the dip has been displaced upwards and the next higher one (the top line) has been pushed down. This suggests that  $V_T/V_0$  should be a function of  $I/I_0$  and  $B/B_0$  also, instead of being taken as a constant for strapped tubes and a function of  $B/B_0$  only for rising sun magnetrons.

### V. CONCLUSIONS

A magnetron model and calculation procedure have been presented that agree tolerably well with observations over a wide range of known tube types. The procedure yields a large amount of detailed information on charge and power distribution in the tube, and on phasing of the spokes. The model has some recognizable deficiencies, which it is hoped will be reduced by further refinement.

### ACKNOWLEDGMENT

The author wishes to thank P. W. Crapuchettes, Technical Director of Litton Electron Tube Division, for his support of this work and for some stimulating discussions of the method. He is indebted to Litton Industries for permission to publish the results.

*Note added in proof:* It has been realized that there is an error in (3) and (4) and in Fig. 1. In each case  $V_{RF}/\sqrt{2}$  should be  $V_{RF}/2$ . The numerical cases are being recalculated. The effect of the change is to leave operation at the Hartree voltage unchanged, but to raise the

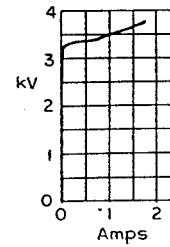


Fig. 11. V-I trace of L-5001 magnetron for comparison with the calculated 1400-Gauss line in Fig. 6.

starting voltage and decrease the dynamic impedance. It thus corrects the problem discussed in Section IV. The author offers his apology for failing to find this error until after the paper was in type and approved.

### REFERENCES

- [1] O. Buneman, "A small-amplitude theory for magnetrons," *J. Electron. Contr.*, no. 1, p. 1, July 1957.
- [2] D. Dunsmuir, "The theory of circular magnetrons with uniformly rotating space charge," presented at the IEE Conv. Microwave Valves, May 1958, Paper 2639.
- [3] S. R. Tibbs and F. I. Wright, CVD Rep., mag. 41, 1945 (British Admiralty).
- [4] S. P. Yu, G. P. Kooyers, and O. Buneman, "Time-dependent computer analysis of electron-wave interaction in crossed fields," *J. Appl. Phys.*, vol. 36, pp. 2550-2559, Aug. 1965.
- [5] H. W. Welch, "Prediction of traveling wave magnetron frequency characteristics," *Proc. IRE*, vol. 41, no. 11, Nov. 1953.
- [6] J. F. Hull, "Crossed-field electron interaction of the distributed-emission space-charge-limited type," *IRE Trans. Electron Devices*, vol. ED-8, pp. 309-323, July 1961.
- [7] J. F. Hull, "Crossed field electron interaction in space charge limited beams," Ph.D. dissertation, Polytechnic Institute of Brooklyn, Brooklyn, N. Y. (Litton Eng. Rep. 1).
- [8] A. Azumi, "Mode instability of magnetrons," *Fujitsu Sci. Tech. J.*, vol. 7, no. 1, Mar. 1971.
- [9] V. B. Bayburin and G. L. Sobolev, "Calculation of space charge fields of a planar magnetron," *Radio Eng. Electron. Phys. (USSR)* (English transl.), vol. 11, pp. 742-750, May 1966; also vol. 12, pp. 440-448, Mar. 1967; also vol. 12, pp. 1493-1498, Sept. 1967.
- [10] G. B. Collins, Ed., *Microwave Magnetrons*, vol. 6 (MIT Radiation Laboratory Series). New York: McGraw-Hill, 1948.
- [11] Rep. Res. Committee Millimeter Waves in Japan, Corona Pub. Co., Tokyo, Japan, 1963, pp. 84-87.
- [12] J. R. M. Vaughan, "A millimetre wave magnetron," *Proc. Inst. Elec. Eng.*, pt. C, monogr. 142R, Aug. 1955.
- [13] R. L. Jepsen and M. W. Muller, "Enhanced emission from magnetron cathodes," *J. Appl. Phys.*, vol. 22, p. 1196, 1951.

Reprinted from IEEE TRANSACTIONS  
ON ELECTRON DEVICES

Volume ED-20, Number 9, September, 1973  
pp. 818-826

COPYRIGHT © 1973—THE INSTITUTE OF ELECTRICAL AND ELECTRONICS ENGINEERS, INC.  
PRINTED IN THE U.S.A.

### Discussion of Incorrect Equations in "A Model for Calculation of Magnetron Performance"

J. RODNEY M. VAUGHAN

**Abstract**—An error in the above-mentioned paper<sup>1</sup> is noted. It is shown that the general conclusions of the paper remain valid, while the accuracy of the calculated dynamic impedance is substantially improved when the error is corrected.

Attention was drawn by a note added in proof to the above paper<sup>1</sup> to an error occurring in two equations and a figure. The common error was not typographical, but occurred in the author's original work. The purpose of this correspondence is to discuss the effect of the error on the conclusions drawn in the paper.

The problem was a confusion in the definition of  $V_{RF}$  between the first part of the analysis, relating the spoke phase to the voltages, and the latter part [(21) on] relating  $V_{RF}$  to the powers, which implied a definition only half that of Fig. 1. Either definition could be changed to secure consistency, but it is simpler to change (3),

(4), and Fig. 1, as indicated in the note appended to the paper. In each case,  $V_{RF}\sqrt{2}$  is replaced by  $V_{RF}/\sqrt{2}$ .

The effect of the correction is quite small, but beneficial. Since the denominator in (3) and (4) is effectively halved, the numerator  $V_H - V_a$  is halved also for a given phase. But because  $V_a$  is always close to  $V_H$ , this only implies a small change in  $V_a$ .

The effect is to rotate each Gauss line a small amount clockwise, pivoting about the point on it where the anode voltage is equal to the Hartree voltage. As this point is always well out along the Gauss line, the effect in the region of normal operation is very small. The agreement of major parameters shown in Table II of the paper is not significantly changed, but the agreement on dynamic impedance and starting voltage, which were listed first in Section IV of the paper as deficiencies of the model, is substantially improved. The major deficiency now left is the excessive jump into oscillation at the higher magnetic fields.

All four of the test cases have been recalculated; the conclusion drawn that the spoke phase is always between  $-60^\circ$  and  $-20^\circ$  is unaltered, but the phase range along a single Gauss line may be as high as  $20^\circ$ ; the discussions of the broad maximum in spoke charge, and of frequency pushing, both remain valid. At the normal operating current, the frequency pushing of the 4J50 now agrees with Hull's measured value within 0.5 MHz. The  $V$ - $I$  diagrams are altered only in minor detail. It does not seem necessary to republish them, since their purpose was not to give specific numerical values, but to show that the mathematical model would generate a reasonable facsimile of the actual performance chart over a wide range of cases. With the correction, the facsimile is modestly improved.

Manuscript received August 20, 1973.  
The author is with Litton Industries, San Carlos, Calif. 94070.  
<sup>1</sup>J. R. M. Vaughan, *IEEE Trans. Electron Devices*, vol. ED-20, pp. 818-826, Sept. 1973.